N-Palmitoyl Sphingomyelin Bilayers: Structure and Interactions with Cholesterol and Dipalmitoylphosphatidylcholine†

P. R. Maulik‡,§ and G. G. Shipley*,§,||

Departments of Biophysics and Biochemistry, Center for Advanced Biomedical Research, Boston University School of Medicine, Boston, Massachusetts 02118

Received November 30, 1995; Revised Manuscript Received March 21, 1996⊗

ABSTRACT: The structure and thermotropic properties of *N*-palmitoyl sphingomyelin (C16:0-SM) and its interaction with cholesterol and dipalmitoylphosphatidylcholine (DPPC) have been studied by differential scanning calorimetry (DSC) and X-ray diffraction methods. DSC of hydrated multi-bilayers of C16:0-SM shows reversible chain-melting transitions. On heating, anhydrous C16:0-SM exhibits an endothermic transition at 75 °C (ΔH = 4.0 kcal/mol). Increasing hydration progressively lowers the transition temperature (T_M) and increases the transition enthalpy (ΔH), until limiting values (T_M = 41 °C, ΔH = 7.5 kcal/mol) are observed for hydration values >25 wt % H_2O. X-ray diffraction at temperatures below (29 °C) T_M show a bilayer gel structure (d = 73.5 Å, sharp 4.2 Å reflection) for C16:0-SM at full hydration; above T_M, at 55 °C, a bilayer liquid-crystal phase is present (d = 66.6 Å, diffuse 4.6 Å reflection). Addition of cholesterol to C16:0-SM bilayers results in a progressive decrease in the enthalpy of the transition at 41 °C, and no cooperative transition is detected at >50 mol % cholesterol. X-ray diffraction shows no difference in the bilayer periodicity, position/width of the wide-angle reflections, or electron density profiles at 29 and 55 °C when 50 mol % cholesterol is present. Thus, cholesterol inserts into C16:0-SM bilayers progressively removing the chain-melting transition and changing the structural characteristics of the bilayer. DSC and X-ray diffraction data show that DPPC is completely miscible with C16:0-SM bilayers in both the gel and liquid-crystalline phases; however, 30 mol % C16:0-SM removes the pre-transition exhibited by DPPC.

INTRODUCTION

Specific molecular blends of phospholipids, glycosphingolipids and cholesterol provide the lipid composition of the bilayer matrix of mammalian cell membranes. The sphingosine-based sphingomyelin (SM)[1] and glycerol-based phosphatidylcholine (PC), together with cholesterol, are major constituents of most mammalian plasma membranes, with SM and PC maintaining an asymmetric disposition across the lipid bilayer. For example, there is convincing evidence for a preferential location of PC and SM on the external monolayer of the erythrocyte membrane. The role and disposition of cholesterol in membranes are not fully understood, but clearly it plays a role in regulating bilayer properties, e.g., membrane fluidity, chain order. This compositionally-heterogeneous lipid bilayer provides both a general permeability barrier and a matrix in which membrane proteins are asymmetrically inserted in order to fulfill their receptor, signaling, transport, and enzymatic functions. Furthermore, the cholesterol-transporting serum lipoproteins, containing a neutral lipid core of cholesterol esters and triglycerides, are surface stabilized by a monolayer of polar SM, PC, and cholesterol; specific apoproteins associated with this surface monolayer provide specific receptor-recognition and enzyme cofactor functions.

It has become clear that at least some phospholipids play a more direct functional role in membranes. Notably, ligand-stimulated membrane receptors activate target membrane enzymes to produce second messengers, which in turn play a key role in the stimulation of basic cellular processes such as cell growth, division, etc. For example, membrane PC hydrolysis by phospholipase A_2 provides the arachidonic acid which is then converted to active prostaglandins, leukotrienes, etc. (Exton, 1994). On the other hand, PI hydrolysis by a PI-specific phospholipase C produces two second messengers, diacylglycerol (Nishizuka, 1984) and inositol triphosphate (Berridge & Irvine, 1989). Finally, hydrolysis of membrane SM by a sphingomyelinase results in the production of ceramide, a structural analogue of diacylglycerol. It has been shown that the released ceramide acts as a second messenger via activation of both protein kinase and protein phosphatase pathways; ultimately, these processes are thought to be involved in the control of both cell growth and apoptosis [for reviews, see Hannun (1994) and Hannun and Obeid (1995)]. Thus, from the viewpoint of both membrane/lipoprotein structure and the functional role of SM in membranes, there is good reason to explore the structure and properties of SM and its interactions with what appear to be its membrane partners, PC and cholesterol.

A variety of physico-chemical techniques have been used to define the structure and properties of natural and synthetic PCs and their interaction with cholesterol. In contrast, much less attention has been paid to SM structure, properties, and interactions. The initial X-ray diffraction study of Reiss-Husson (1967) showed that hydrated bovine brain SM

† This research was supported by Research Grant HL-26335 and Training Grant HL-07291 from the National Institutes of Health.

* Author to whom correspondence should be addressed.

‡ Present address: Central Drug Research Institute, Lucknow-22601, India.

§ Department of Biophysics.

|| Department of Biochemistry.

⊗ Abstract published in *Advance ACS Abstracts,* May 15, 1996.

[1] Abbreviations: DSC, differential scanning calorimetry; SM, sphingomyelin; PC, phosphatidylcholine; DPPC, dipalmitoylphosphatidylcholine; SPC, sphingosylphosphorylcholine.

S0006-2960(95)02835-2 CCC: $12.00

exhibited a gel phase at 25 °C and liquid-crystalline phase at 40 °C. Our own study (Shipley et al., 1974) using DSC and X-ray diffraction showed that bovine brain SM (rich in C18:0 and C24:1 fatty acids) formed hydrated bilayers which undergo a complex gel to liquid-crystal phase transition with maxima at 34 and 38 °C. Similar thermotropic behavior was demonstrated by Barenholz et al. (1976) in their calorimetric study of bovine brain SM. Studies of binary mixtures of bovine brain SM with egg yolk PC revealed bilayer phase separation of the high-melting SM (Untracht & Shipley, 1977), whereas in the bovine brain SM-cholesterol binary system cholesterol progressively removed the SM transition [L. S. Avecilla and G. G. Shipley, unpublished observations; also, see Oldfield and Chapman (1972) and McIntosh et al. (1992a)].

Natural SM (e.g., bovine brain SM) is compositionally-heterogeneous in terms of both its amide-linked fatty acid and, to a lesser extent, its sphingosine base (Calhoun & Shipley, 1979a). Therefore, starting with bovine brain SM, we synthesized C16:0-SM using a deacylation−reacylation protocol and showed that in miscible C16:0-SM/DMPC bilayers cholesterol had no preferential affinity for SM over PC (Calhoun & Shipley, 1979b). This contrasted with earlier studies indicating that in immiscible binary phospholipid systems cholesterol had a preference for certain phospholipids and that cholesterol had the highest affinity for SM (van Dijck et al., 1976; Demel et al., 1977). We then synthesized a series of SM with specific (C14:0, C16:0, C18:0, C20:0, C22:0, C24:0, and C24:1) fatty acyl chains (Sripada et al., 1987). Initial DSC studies indicated that whereas C16:0-, C18:0-, and C20:0-SM show simple thermotropic behavior with a single chain-melting transition, the longer chain (C22:0- and C24:0-SM) and shorter chain (C14:0-SM) sphingomyelins exhibit several transitions. Mismatch in the length of the sphingosine (C18) and N-acyl chains is likely to be responsible for the more complex gel [and perhaps liquid-crystal L_α: see Maulik et al. (1986)] strutural behavior. Recently, we have described the structural changes underlying the thermotropic behavior of C18:0-SM (Maulik et al., 1991) and C24:0-SM (Maulik & Shipley, 1995).

An alternative strategy has involved the *de novo* synthesis of chemically pure SM. Several protocols have been described for the synthesis of stereochemically pure D-*erythro*- and L-*threo*-SM, as well as racemic DL-*erythro* SM (Shapiro & Flowers, 1962; Bruzik, 1988; Kratzer et al., 1993; Dong & Butcher, 1993). Barenholz and colleagues (1976; Estep et al., 1979, 1981) have described the thermotropic properties of fully hydrated DL-*erythro* C16:0-, C18:0-, and C24:0-SM and their interactions with cholesterol. Whereas C18:0- and C24:0-SM exhibited two thermal transitions, only a single, reversible transition at ∼41 °C is observed for C16:0-SM. In all cases, addition of cholesterol removed the SM phase transition(s) but at intermediate cholesterol contents the presence of cholesterol-rich and cholesterol-poor domains was inferred (Estep et al., 1979, 1981). Later, Bruzik and Tsai (1987) compared the thermotropic behavior of D-*erythro* and L-*threo* C18:0-SM; while their chain-melting temperatures were essentially identical (44−45 °C), the stereoisomers exhibited different bilayer gel phases particularly when subjected to low-temperature incubation.

In the present study, we use DSC and X-ray diffraction to provide a detailed description of (i) the structure, hydration, and thermotropic properties of C16:0-SM and (ii) the interaction of C16:0-SM with cholesterol and DPPC.

MATERIALS AND METHODS

Materials. *N*-Palmitoylsphingomyelin (C16:0-SM) was synthesized from bovine brain SM (Calbiochem-Behring Diagnostic, San Diego, CA) as described previously (Sripada et al., 1987). Briefly, acid hydrolysis of bovine brain SM containing heterogeneous N-acyl chains produced sphingosylphosphorylcholine (SPC). C16:0-SM was obtained after reacylation of SPC using palmitoyl imidazolide to *O*-*N*-dipalmitoyl SPC, followed by hydrolysis of the *O*-ester bond. The resulting C16:0-SM was shown to be >99% pure by a combination of thin-layer chromatography and high-performance liquid chromatography. However, as noted previously (Sripada et al., 1987; Maulik et al., 1991; Maulik & Shipley, 1995), epimerization at C-3 of sphingosine does occur during the acid hydrolysis step, leading to the formation of some of the L-*threo* stereoisomer of SPC. Because we have not been able to separate the stereoisomers of either SPC or the reacylated SM, the desired product D-*erythro*-SM, does contain ∼25% of the L-*threo* isomer [for a detailed discussion of this issue for C16:0-SM, see Sripada et al. (1987)]. For the starting material, bovine brain SM, the predominant sphingosine base is C18:1t (90.2%) plus minor amounts of C20:1t (7.3%) and C18:0 (2.6%). In our detailed study of C16:0-SM (Sripada et al., 1987), C18:1t is retained as the major sphingosine base (85.7%), with changes occurring in the levels of the minor sphingosine components.

Cholesterol (Nu Chek Prep, Austin, MN) and DPPC (Avanti Polar Lipids, Birmingham, AL) were shown to be >99% pure by thin-layer chromatography using the following solvent systems: cholesterol, hexane/ethyl ether/acetic acid (70:30:1 v/v); DPPC, chloroform/methanol/water/acetic acid (65:25:4:1 v/v).

Differential Scanning Calorimetry. Samples of C16:0-SM were weighed into stainless steel DSC pans, and the calculated amount of doubly distilled water was added by a Hamilton syringe to give various hydration states of C16:0-SM. C16:0-SM with various molar ratios of cholesterol or DPPC was directly weighed into DSC pans and dissolved in chloroform−methanol (2:1, v/v). The solvent was evaporated under a slow nitrogen stream, and the sample was placed in a vacuum overnight. The DSC pans were reweighed to make sure that the total amount of lipids remains constant. Doubly distilled water was added using a Hamilton microsyringe to make binary mixtures of C16:0-SM/cholesterol and C16:0-SM/DPPC in excess (75 wt %) water. The DSC pans were then hermetically sealed.

The DSC sample pans were placed in a Perkin Elmer DSC-2 calorimeter (Norwalk, CT). Heating and cooling scans at 5 °C/min were recorded during repeated cycling over the temperature range 0−87 °C. The peak maximum in the plot of excess heat capacity vs temperature was recorded as the transition temperature, T_M; the transition enthalpy was derived from the area under the transition as measured by planimetry and compared with the known enthalpy of a standard (gallium).

X-ray Diffraction. Samples of anhydrous C16:0-SM were weighed directly into quartz capillaries (i.d. = 1.0 mm). The desired amount of doubly distilled water was added by microsyringe, and the capillary tubes were flame-sealed immediately. The capillaries were centrifuged several times at temperatures 10 °C above the transition temperature in order to achieve equilibration. C16:0-SM with various molar ratios of cholesterol or DPPC was weighed into glass tubes

with a central constriction. The lipids were then dissolved in chloroform−methanol (2:1, v/v), the solvent was evaporated under nitrogen, and the sample was placed in a vacuum overnight. The tubes were then reweighed to check for lipid loss. Doubly distilled water was added using a Hamilton microsyringe to make the binary lipid mixtures in excess water (50 wt %), and the tube was immediately flame-sealed. Sample equilibration was achieved by repeated centrifugation of the sample through the central constriction for 4−5 h at 10 °C above the phase transition temperature. The sample tubes were then opened, samples were promptly transferred to X-ray diffraction quartz capillary tubes, and the capillaries were flame-sealed immediately.

The capillaries containing hydrated lipids were placed in variable-temperature sample holders. X-ray diffraction patterns were recorded on focussing cameras with either toroidal mirror (Elliott, 1965) or double-mirror (Franks, 1958) optics using Ni-filtered Cu Kα ($\lambda = 1.5418$ Å) radiation from an Elliot GX-6 rotating anode generator (Elliot Automation, Borehamwood, U.K.). The temperature of the sample holder was kept constant by a circulating solvent/water bath. The diffraction intensities were measured using a Joyce-Loebl (Gateshead, U.K.) model III-CS scanning microdensitometer. X-ray diffraction patterns were also recorded with a position-sensitive linear detector (Tennelec, Oak Ridge, TN) and associated electronics (Tracor Northern, Middleton, WI). Ni-filtered Cu Kα ($\lambda = 1.5418$ Å) radiation from a microfocus X-ray generator (Jarrel-Ash, Waltham, MA) was line focused by a single mirror and collimated with the slit optical system of a Luzzati−Baro camera (E^{TS} Beaudoin, Paris, France).

RESULTS

Hydrated C16:0-SM. DSC heating scans (5 °C/min) for C16:0-SM at different hydrations were recorded over the temperature range 0−87 °C (Figure 1). Following equilibration, the initial heating scan followed by immediate cooling and second heating scans (i.e., without high- or low-temperature incubation, respectively) confirmed the reversible nature of the transition at all hydrations. In the absence of water, C16:0-SM shows an endothermic transition at 75 °C ($\Delta H = 4.0$ kcal/mol C16:0-SM). As the hydration increases, the transition temperature T_M (Figure 2a) decreases and the transition enthalpy (Figure 2b) increases, reaching limiting values ($T_M = 41$ °C; $\Delta H = 7.5$ kcal/mol) at hydration levels >22 wt % H_2O. At low hydration levels (5.2, 9.4, and 16.0 wt % H_2O), the chain-melting transition is quite broad and low-enthalpy sub-transitions are observed at 25−30 °C ($\Delta H \approx 0.3$ kcal/mol). However, incubation of these C16:0-SM samples at 4 °C for up to 48 h does not increase the enthalpy of the sub-transitions (data not shown).

X-ray diffraction patterns of hydrated (10−50 wt % H_2O) C16:0-SM were recorded at temperatures below (29 °C) and above (55 °C) the observed calorimetric transition, T_M (see Figures 1 and 2). At 29 °C, C16:0-SM at all hydration levels showed a series of lamellar low-angle reflections and a single, fairly sharp, wide-angle reflection at ∼4.2 Å. For example, the diffraction pattern for fully hydrated (50 wt % H_2O) C16:0-SM shows lamellar reflections ($h = 1-4$) corresponding to a bilayer periodicity $d = 73.5$ Å, together with a sharp 4.2 Å reflection indicative of quasihexagonal hydrocarbon chain packing. At 55 °C, the diffraction pattern at all hydration levels (with the exception of 10 wt % H_2O, see below) also gave a series of lamellar low-angle reflections

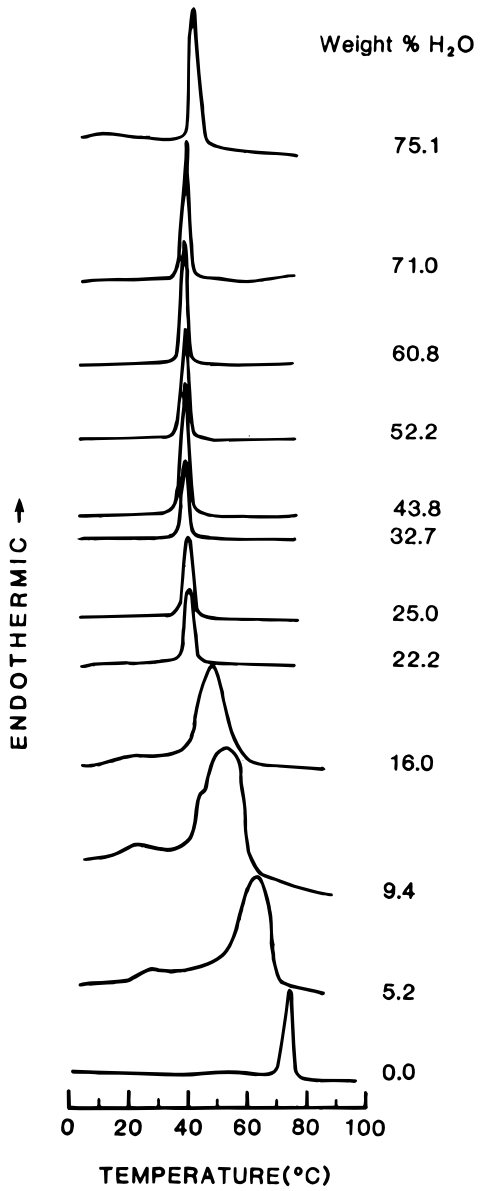

FIGURE 1: DSC heating scans of C16:0-SM at different hydrations; heating rate, 5 °C/min.

but a diffuse wide-angle reflection at ∼4.6 Å. For fully hydrated (50 wt % H_2O) C16:0-SM the bilayer periodicity $d = 65.9$ Å, with the broad 4.6 Å reflection confirming the melted chain state. These X-ray diffraction patterns are typical of those observed for hydrated phospholipid bilayers in the gel phase with hexagonal chain packing and the liquid-crystalline phase with disordered chains, respectively. At 29 and 55 °C, the positions and relative intensities of the low-angle reflections change on increasing hydration up to 24.0 and 22.5 wt % H_2O, respectively (see below).

Figure 3 shows the temperature dependence of the diffraction pattern of hydrated C16:0-SM (30 wt % H_2O) recorded with the position sensitive detector. The diffraction pattern showing the lamellar reflections $h = 2-4$ the wide-angle region recorded at 4° increments over the temperature range 12−68 °C is shown in Figure 3 (right). The low-angle region was recorded at higher resolution at 3° intervals and shows the temperature dependence of the lamellar reflections $h = 1-3$ (Figure 3, left). At 12 °C, the bilayer periodicity is 71.0 Å and a sharp reflection at 4.16 Å is observed. No significant changes are observed over the temperature range 12−40 °C. However, both the low- and

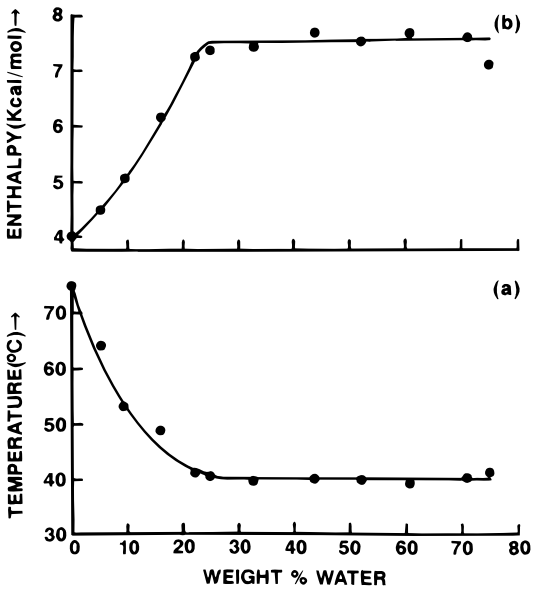

FIGURE 2: Transition temperature T_M (a) and transition enthalpy (b) of C16:0-SM as a function of hydration.

wide-angle regions exhibit changes at ~40−45 °C, reflecting a decrease in bilayer periodicity and a change in the chain packing, respectively. At 55 °C, the bilayer periodicity is reduced to 65.6 Å and the broad wide-angle reflection at 4.5 Å is obvious.

A plot of bilayer periodicity (d) as a function of hydration is shown in Figure 4. At 29 °C, C16:0-SM bilayers hydrate over the hydration range 10−24 wt % H_2O, the bilayer periodicity, d, increasing from 60.4 to 73.5 Å; no further change in d is observed at >24 wt % H_2O, thus defining the hydration limit of gel phase of C16:0-SM (Figure 4, left). At 55 °C, over the hydration range 15−22.5 wt % H_2O, the bilayer liquid-crystal phase of C16:0-SM exhibits swelling, d increasing from 58.6 to 66.0 Å (Figure 4, right). For water contents >22.5 wt % H_2O, no further swelling is observed. For 10 wt % H_2O, at 55 °C C16:0-SM is still in the gel phase. Therefore, an X-ray diffraction pattern was also recorded at 70 °C, i.e., in the liquid-crystalline phase. The measured bilayer periodicity, d = 53.8 Å, agrees well with the extrapolated data at 55 °C (see Figure 4, right).

The bilayer thickness (d_1) and the area (S) per molecule at the lipid−water interface were also calculated at 22 °C (gel phase) and 55 °C (liquid-crystal phase) at different hydrations using the Luzzati formalism (Luzzati, 1968). The partial specific volumes (υ_1) for C16:0-SM were assumed to be 0.945 mL/g at 29 °C and 1.012 mL/g at 55 °C, corresponding to values determined for similar phases of dipalmitoyl PC (Nagle & Wilkinson, 1978). The molecular weight of C16:0-SM was 703.0. The calculated values of the structural parameters d_1 and S of C16:0-SM at 29 and 55 °C are also plotted in Figure 4. In the gel phase at 29 °C, d_1 (=54 Å) and S (=41 Å^2) are essentially independent of hydration; similarly at 55 °C in the liquid-crystalline phase, d_1 (=51 Å) and S (=47 Å^2) show little hydration dependence.

To derive additional structural information for C16:0-SM bilayers, the intensities of the lamellar low-angle reflections at different hydrations were measured, corrected, and converted into structure amplitudes, and then hydration sets were scaled (Worthington & Blaurock, 1969). Phases were derived from the plotted amplitude data for all hydration sets (the swelling method) as described previously [for example, see Torbet and Wilkins (1976), Janiak et al. (1979), McIntosh and Simon (1986), Maulik et al. (1991), and Maulik and Shipley (1995)]. The phased amplitudes were used to calculate electron density profiles at each hydration. Figure 5 shows the electron density profiles of C16:0-SM bilayers at 29 °C (left) and 55 °C (right) at different hydration states. The profiles consist in all cases of a central trough (corresponding to the bilayer center) separating two peaks of high electron density (locating the electron dense phosphate groups of C16:0-SM); the profiles at lower hydration show additional detail. The peak separation across the bilayer provides another measure of the bilayer thickness, d_{p-p}, and is plotted as a function of C16:0-SM hydration in Figure 4. The thickness of the inter-bilayer hydration layer d_w is given by $d_w = d - d_{p-p}$. For both the gel (29 °C) and liquid-crystalline (55 °C) phases the bilayer thickness is essentially hydration-independent with d_{p-p} values of 48 and 42 Å, respectively (Figures 4 and 5).

C16:0-SM−Cholesterol Interactions. The interaction of C16:0-SM and cholesterol in excess water was investigated by DSC and X-ray diffraction methods. Figure 6 shows the DSC heating curves of fully hydrated (75 wt % H_2O) C16:0-SM containing increasing mol % cholesterol. C16:0-SM exhibits a sharp endothermic transition at 41 °C. As the cholesterol content increases, the C16:0-SM transition progressively decreases in enthalpy and increases in transition width. Finally, at cholesterol contents ≥50 mol % no cooperative transition is detected. The total transition enthalpy plotted as a function of mol % cholesterol is shown in Figure 7. Over the range 0−20 mol % cholesterol the transition enthalpy is reduced linearly with increasing cholesterol content but at higher cholesterol contents when the residual transition is extremely broad a more complex dependence is observed (Figure 7).

X-ray diffraction data of hydrated (50 wt %) C16:0-SM containing increasing mol % cholesterol (0−60 mol % cholesterol) were recorded at 29 and 55 °C, i.e., below and above the transition of hydrated C16:0-SM. All diffraction patterns exhibited lamellar geometry, indicating the presence of bilayer structure at both temperatures and at all cholesterol contents. The bilayer periodicity (d) is shown as a function of mol % cholesterol in Figure 8. At 29 °C, the bilayer periodicity (d) in the absence of cholesterol is 73.5 Å. With increasing cholesterol content d decreases linearly until a limiting value of 63.7 Å is reached at 50 mol % cholesterol. At 50 °C, bilayer periodicity is less dependent on cholesterol content than at 29 °C, decreasing from 66.6 to 63.3 Å at 50 mol % cholesterol. X-ray diffraction patterns of hydrated C16:0-SM containing 50 mol % cholesterol at 29 °C (bottom) and 55 °C (top) are shown in Figure 9. The diffraction patterns are essentially identical in bilayer periodicity (64 Å), as well as position (4.7 Å) and width of the wide-angle reflection. At 29 °C, these data clearly demonstrate progressive perturbation by cholesterol of the original bilayer structure (periodicity and chain packing) of the bilayer gel phase of C16:0-SM. We have also calculated electron density profiles from the X-ray diffraction data of C16:0-SM at 50 mol % cholesterol; the profiles at 29 and 55 °C (Figure 10, bottom) are compared with those of C16:0-SM alone (Figure 10, top). Given the similarity of the diffraction patterns (Figure 9), predictably in the presence of 50 mol % cholesterol, the profiles are essentially identical at 29 and 55 °C in terms of both the bilayer thickness (d_{p-p} = 45.2 Å) and the hydration layer thickness (~9 Å) (Figure 10, bottom). Comparison with the profiles of C16:0-SM shows that at 29

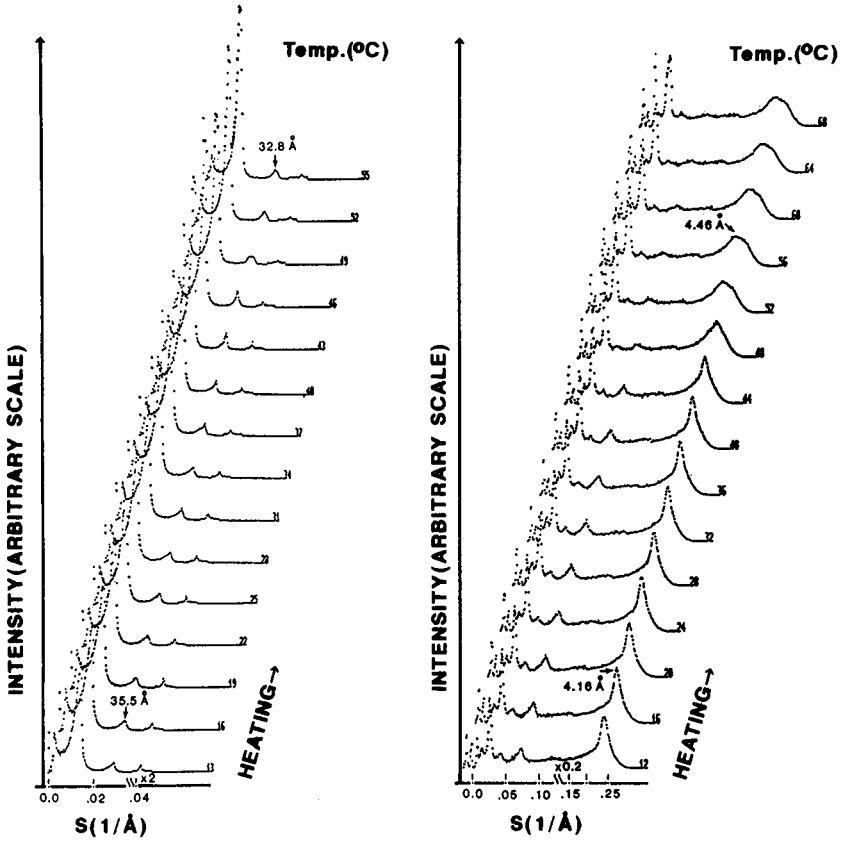

FIGURE 3: X-ray diffraction patterns of hydrated (30 wt % H_2O) C16:0-SM as a function of temperature recorded using a position sensitive detector. Left, low-angle region; right, wide-angle region.

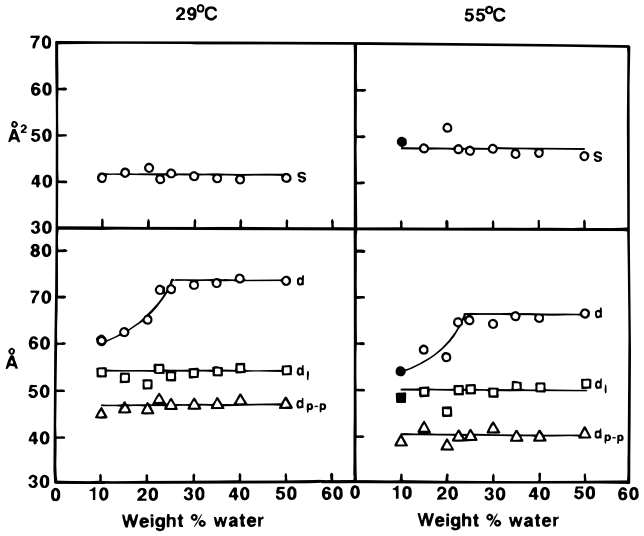

FIGURE 4: Bilayer parameters of C16:0-SM as a function of hydration at 29 °C (left) and 55 °C (right). Lower panels: (○) bilayer periodicity, d (Å); (□) lipid thickness, d_l (Å); (△) phosphate−phosphate separation from electron density profiles, d_{p-p} (Å); filled symbols, data at 70 °C. Upper panels: (○) surface area per C16:0-SM molecule at the lipid−water interface, S (Å^2).

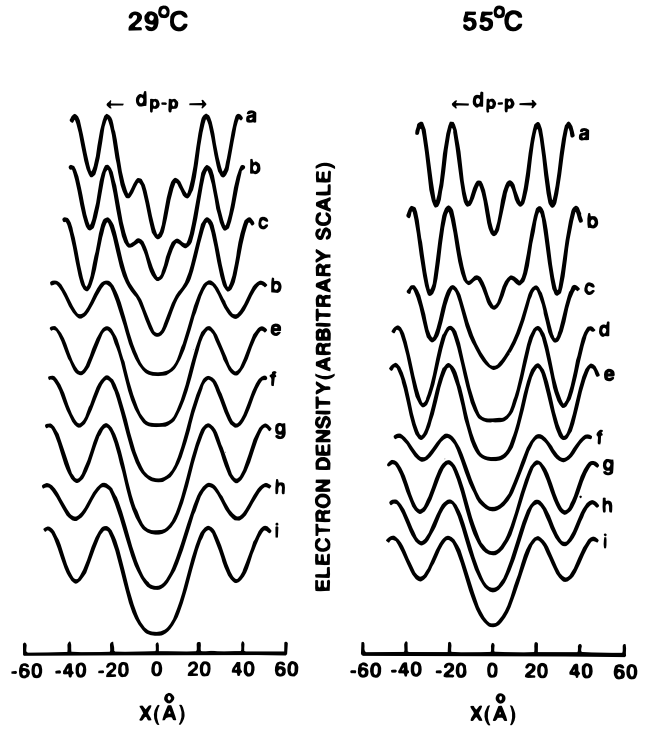

FIGURE 5: Electron density profiles of C16:0-SM bilayers at different hydrations: left, 29 °C; right, 55 °C. (a) 10, (b) 15, (c) 20, (d) 22.5, (e) 25, (f) 30, (g) 35, (h) 40, and (i) 50 wt % H_2O.

°C the bilayer thickness decreases from 49.6 to 45.2 Å on incorporation of 50 mol % cholesterol; at 55 °C, a small increase in d_{p-p} (from 44.4 to 45.2 Å) is observed. The location of cholesterol in the bilayer is indicated by the additional electron density in the profiles at ±10 Å. Thus, it is clear that cholesterol incorporation induces structural changes in C16:0-SM bilayers.

C16:0-SM/DPPC Interactions. DSC heating scans of hydrated (75 wt % H_2O) C16:0-SM containing increasing mol % DPPC are shown in Figure 11. The chain-melting transition of C16:0-SM occurs at 41 °C (ΔH = 7.5 kcal/mol); with increasing DPPC content, the transition temperature decreases slightly (0−20 mol %), remains constant at 37 °C (20−70 mol %), and then increases slightly (70−100 mol %) to the chain-melting transition temperature of DPPC, 41.5 °C (Figure 11 and Figure 12, bottom). The transition

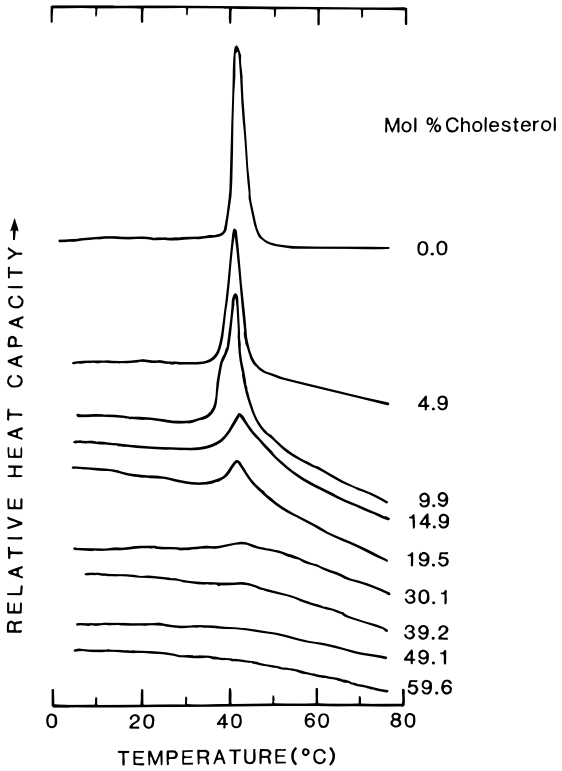

FIGURE 6: DSC heating scans of hydrated (75 wt % H_2O) C16:0-SM containing increasing mol % cholesterol; heating rate, 5 °C/min.

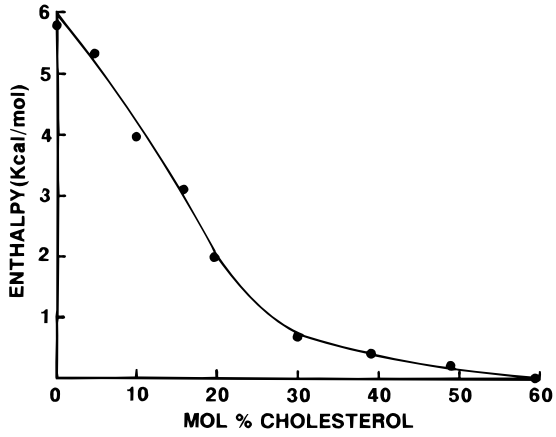

FIGURE 7: Transition enthalpy of hydrated C16:0-SM/cholesterol mixtures as a function of cholesterol content.

enthalpy increases linearly with increasing DPPC content over the range 10−100 mol % DPPC (Figure 12, top). In the range 0−70 mol % DPPC, a single reversible chain-melting transition is observed, but at >70 mol % DPPC the pre-transition characteristic of DPPC is observed (Figure 11). Increases are observed in the pre-transition temperature (27−34 °C) and enthalpy (0.4−1.02 kcal/mol) over the range 80−100 mol % DPPC (Figures 11 and 12). This calorimetric behavior suggests that C16:0-SM and DPPC exhibit miscibility in both the gel and liquid-crystalline bilayer phases. X-ray diffraction data of C16:0-SM containing 25 and 80 mol % DPPC were recorded below and above the calorimetrically-observed transitions. For both binary mixtures, only a single set of lamellar reflections was observed at either 29 or 55 °C (data not shown), thus confirming the miscibility of DPPC in C16:0-SM bilayers.

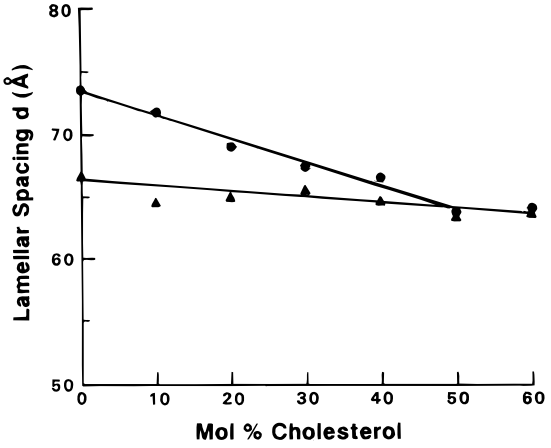

FIGURE 8: Bilayer periodicity, *d*, of hydrated C16:0-SM as a function of cholesterol content: (●) 29 °C; (▲) 55 °C.

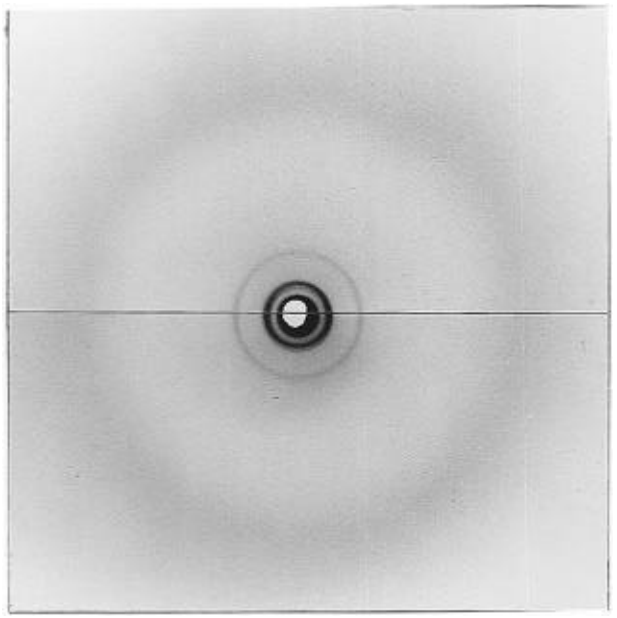

FIGURE 9: X-ray diffraction patterns of hydrated (50 wt % H_2O) C16:0-SM containing 50 mol % cholesterol at 29 °C (bottom) and 55 °C (top); recorded using toroidal X-ray optics.

DISCUSSION

Early calorimetric studies of SM isolated from brain tissue, red cells, egg yolk, etc., in general revealed complex thermotropic behavior due to broad, overlapping transitions (Shipley et al., 1974; Barenholz et al., 1976; Calhoun & Shipley, 1979a). This complex behavior presumably arises from the heterogeneity in their amide-linked fatty acid composition (Calhoun & Shipley, 1979a). A subsequent DSC study of hydrated C16:0-SM synthesized from bovine brain SM deacylation−reacylation methods demonstrated much simpler thermotropic behavior; a single, sharp transition at 41 °C is observed (Calhoun & Shipley, 1979b). We then used the same partial synthesis method to synthesize a series of SM in which the N-acyl chain was varied from C14:0 to C24:0 (Sripada et al., 1987). DSC studies of this series of SM revealed simple thermotropic behavior for C16:0-, C18:0-, and C20:0-SM, whereas the shorter chain (C14:0) and longer chain (C22:0 and C24:0) SM exhibited multiple transitions (Sripada et al., 1987). We have described the structure and properties of C18:0- and C24:0-SM (Maulik et al., 1991; Maulik & Shipley, 1995), focusing on their hydration dependence. In this paper, we extend this approach

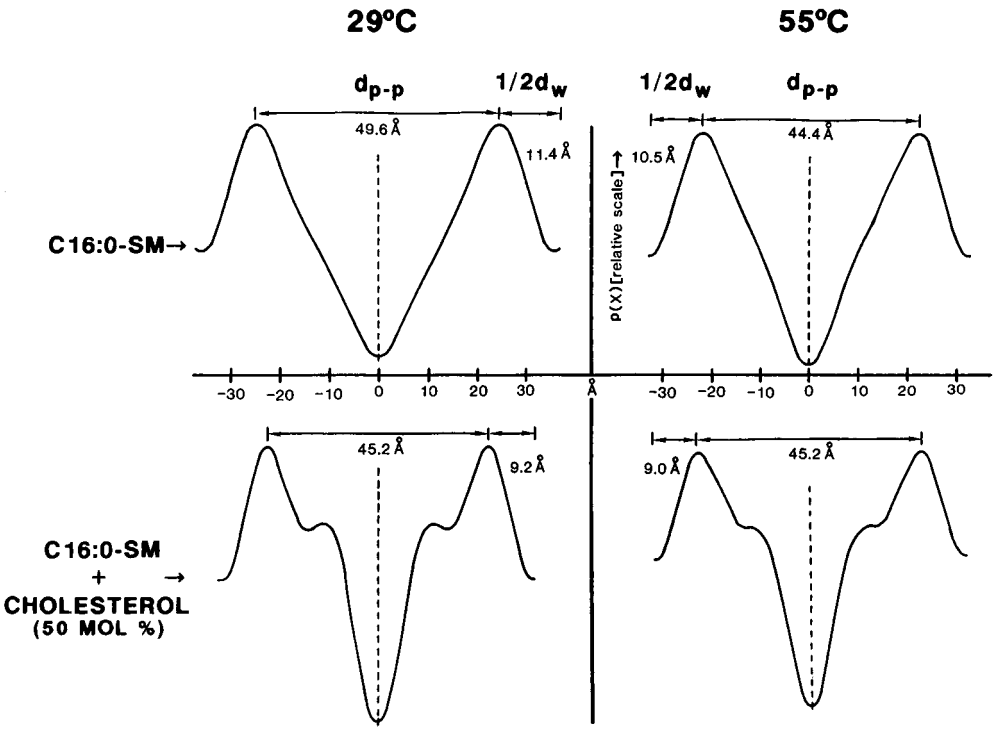

FIGURE 10: Electron density profiles of hydrated C16:0-SM (top) and C16:0-SM/cholesterol (50 mol %) (bottom) at 29 °C (left) and 55 °C (right).

to C16:0-SM, describing its structure, hydration, and thermotropic behavior. In addition, we explore in more detail the interaction of C16:0-SM with cholesterol and DPPC.

C16:0-SM Hydration. Apart from the low-enthalpy subtransitions observed at low hydrations (not explored further), C16:0-SM exhibits quite simple thermotropic behavior. Over the hydration range 0−20 wt % water the chain-melting transition temperature decreases from 75 to 41 °C (Figures 1 and 2); concomitantly, the transition enthalpy increases from 4.0 to 7.5 kcal/mol (Figure 2). The transition temperature agrees well with that described previously for C16:0-SM (40.5 °C; Calhoun & Shipley, 1979b) and DL-*erythro* C16:0-SM (41 °C; Estep et al., 1979). The X-ray diffraction data (Figures 3−5) demonstrate that C16:0-SM forms hydrated lamellar bilayer phases at all hydration levels both below and above its chain-melting transition. At 29 °C, the bilayer gel phase of C16:0-SM (with pseudohexagonal chain packing based on the single 4.2 Å wide-angle reflection) shows a hydration limit corresponding to 24 wt % water (12 H_2O molecules per C16:0-SM molecule) whereas at 55 °C, the hydration limit for the liquid-crystalline L_α phase is 22 wt % H_2O (11 H_2O/C16:0-SM). For fully hydrated C16:0-SM (>24 wt % H_2O), the chain-melting transition is accompanied by the following structural changes: the bilayer periodicity, d, decreases from 71.5 to 64.5 Å; the bilayer thickness decreases, d_1 from 54 to 50 Å, d_{p-p} from 48 to 42 Å; surface area/C16:0-SM increases from 41 to 47 Å^2. Thus, as observed previously for many other phospholipid bilayers, the chain-melting transition is accompanied by a decrease in bilayer thickness, an increase in interfacial molecular area, and a small decrease in both the hydration limit ($\Delta = 2$ wt % H_2O) and the thickness of the hydration layer ($\Delta = 2$ Å).

The structural changes exhibited by C16:0-SM on chain-melting are shown schematically in Figure 13 (left). It should be noted that although C16:0-SM has a C16:0 N-linked chain and a C18:1t (primarily) sphingosine chain, the first three carbons (C1−C3) of the C18 sphingosine are the structural equivalent of the three glycerol carbons of glycerophospholipids such as PC and C4 would be the equivalent of the ester oxygen. Thus, C16:0-SM probably resembles a PC with a C14:0 chain at *sn*-1 and a C16:0 chain at *sn*-2. Further, if the conformation of the interfacial region of SM resembles that of glycerolipids such as phosphatidylethanolamine or PC (Hitchcock et al., 1974; Elder et al., 1977; Pearson & Pascher, 1979; Seelig & Seelig, 1980), then the two chain termini (sphingosine and N-acyl) are probably well matched at the bilayer center for both C16:0-SM, as indicated in Figure 13, and C18:0-SM. Previously, we have presented data supporting this conclusion: (i) DSC data of the series C14:0- to C24:0-SM show "simple", reversible chain-melting transitions for C16:0-, C18:0-, and C20:0-SM and no evidence of gel phase polymorphism, whereas the longer chain (C22:0- and C24:0-SM) and shorter chain (C14:0-SM) SM exhibit multiple transitions indicative of gel phase polymorphism (Sripada et al., 1987); (ii) X-ray diffraction studies of both the gel and L_α phases of C18:0-SM (Maulik et al., 1991) and C16:0-SM (this study) confirm the presence of only a single and, we believe, not interdigitated gel phase, in marked contrast to X-ray diffraction studies of C24:0-SM (Maulik & Shipley, 1995) which reveal two gel phases, at least one of which is partially interdigitated; and (iii) in single-bilayer vesicles, X-ray scattering measurements of bilayer thickness of the L_α phase again suggest little or no chain interdigitation for C16:0- and C18:0-SM but significant interdigitation even of melted chains of C24:0-SM (Maulik et al., 1986). Thus, we conclude that for C16:0- and C18:0-SM the chains are well matched in length and that chain interdigitation across the bilayer center does not occur to a significant extent (Figure 13).

Interestingly, for the three synthetic SM we have examined [C16:0-SM, this paper; C18:0-SM, Maulik et al. (1991); and C24:0-SM, Maulik and Shipley (1995)], the chain-melting transition, T_M, increases progressively with increasing chain

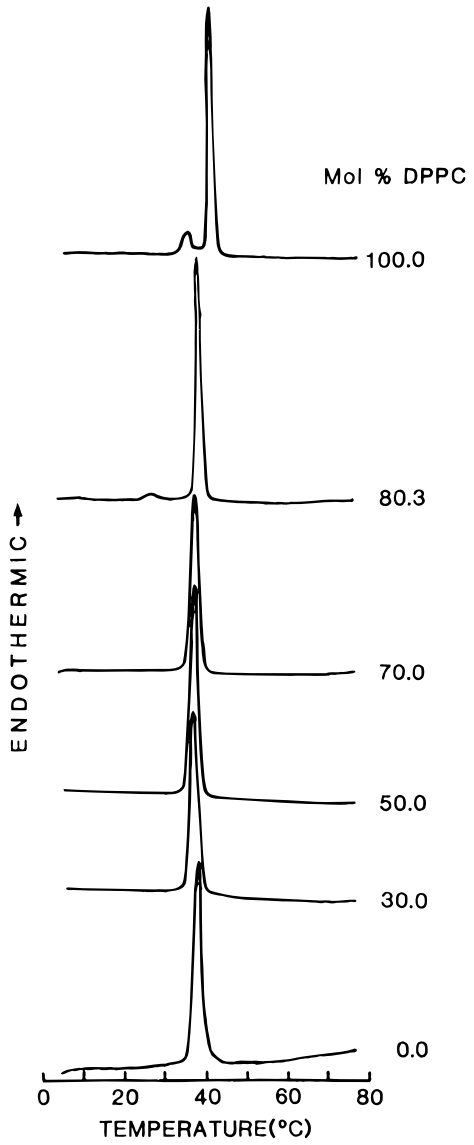

FIGURE 11: DSC heating scans of hydrated (75 wt % H_2O) C16:0-SM containing increasing mol % DPPC; heating rate, 5 °C/min.

length (T_M = 42, 45, and 48 °C, respectively) as predicted but the enthalpy *decreases* with increasing chain length (ΔH = 7.5, 6.7, and 6.1 kcal/mol, respectively). We have three remaining members of the series (C14:0-, C20:0-, and C22:0-SM) to characterize, at which point an evaluation of the chain length dependence, and a comparison with the incisive analysis of an extensive series of mixed-chain PCs (Huang, 1991; Lin et al., 1990, 1991), should be possible. However, the gel phase polymorphism of SM, already characterized for C24:0-SM (Maulik & Shipley, 1995), may prove to be a complicating factor in such comparisons.

C16:0-SM/Cholesterol Interactions. Although less attention has been paid to the interaction of cholesterol with SM, early ^{1}H-NMR and ESR studies (Oldfield & Chapman, 1971, 1972) indicated that cholesterol regulates the fluidity of bovine brain SM bilayers, an effect similar to that observed for PC-cholesterol systems. On the basis of DSC studies, Estep et al. (1979, 1981) suggested that binary mixtures of synthetic C16:0-, C18:0, and C24:0-SM with cholesterol exhibit phase separation with the coexistence of SM-enriched and cholesterol-enriched bilayer phases. Our previous DSC studies showed that cholesterol progressively broadened and removed the chain-melting transition of C16:0-SM, but the main focus of this study was to show that cholesterol did not interact selectively with SM in a miscible SM-PC bilayer (Calhoun & Shipley, 1979b). Recently, McIntosh et al. (1992a) have shown that the presence of 50 mol % cholesterol removes the chain-melting transitions exhibited by both bovine brain SM and partially synthetic C24:0-SM.

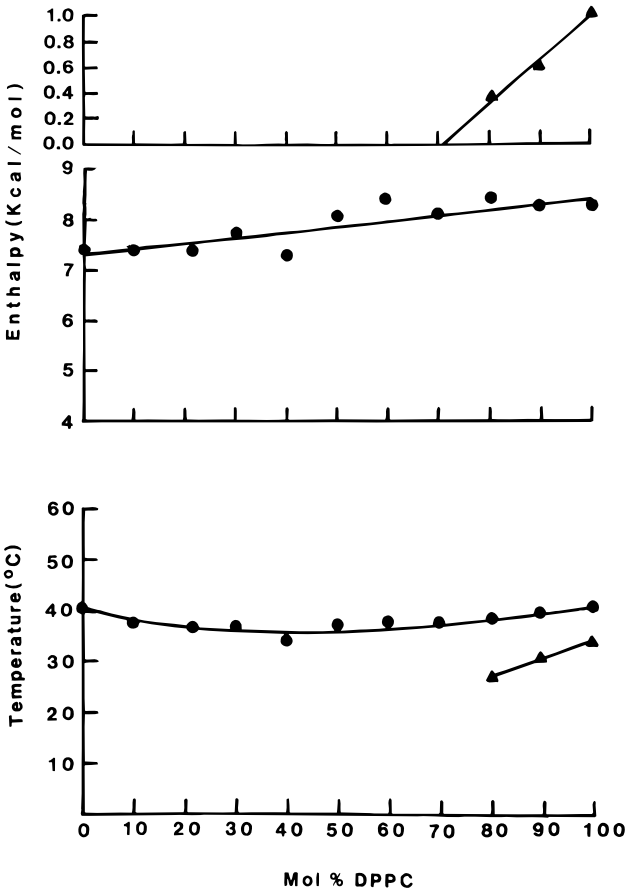

FIGURE 12: Transition temperature (bottom) and enthalpy (top) of hydrated C16:0-SM/DPPC binary mixtures as a function of mol % DPPC. Chain-melting transition, T_M (●); pre-transition, T_p (▲).

Our present calorimetric data (Figures 6 and 7) show that there is a progressive decrease in enthalpy of the chain-melting transition of C16:0-SM as the cholesterol content is increased. Consistent with previous studies of C16:0-SM (Calhoun & Shipley, 1979b) and C24:0-SM (McIntosh et al., 1992a), there is no transition detectable at cholesterol contents ≥50 mol %. The X-ray diffraction data (Figures 8−10) demonstrate that lamellar bilayer phases are present at all C16:0-SM/cholesterol molar ratios. At 29 °C the bilayer periodicity decreases linearly with increasing cholesterol content, and at 50 mol % cholesterol is identical to that observed at 55 °C (Figure 8). This reduction in bilayer periodicity is presumably due to a combination of cholesterol-induced thinning of the bilayer (due to chain disorder effects, see below) and, possibly, hydration layers. At 55 °C the bilayer periodicity is much less dependent on cholesterol content (Figure 8). Electron density profiles of hydrated C16:0-SM containing 50 mol % cholesterol at temperatures below (29 °C) and above (55 °C) the original transition temperature of C16:0-SM are clearly identical in both their overall shape, particularly the cholesterol-associated peak at ±10 Å [also, see McIntosh et al. (1992a,b)] and the derived lipid (d_{p-p} = 45 Å) and water (18 Å) layer thicknesses (Figure 10). Comparison of the profiles in the absence and presence of cholesterol shows that incorporation of cholesterol decreases the bilayer thickness of the original gel phase

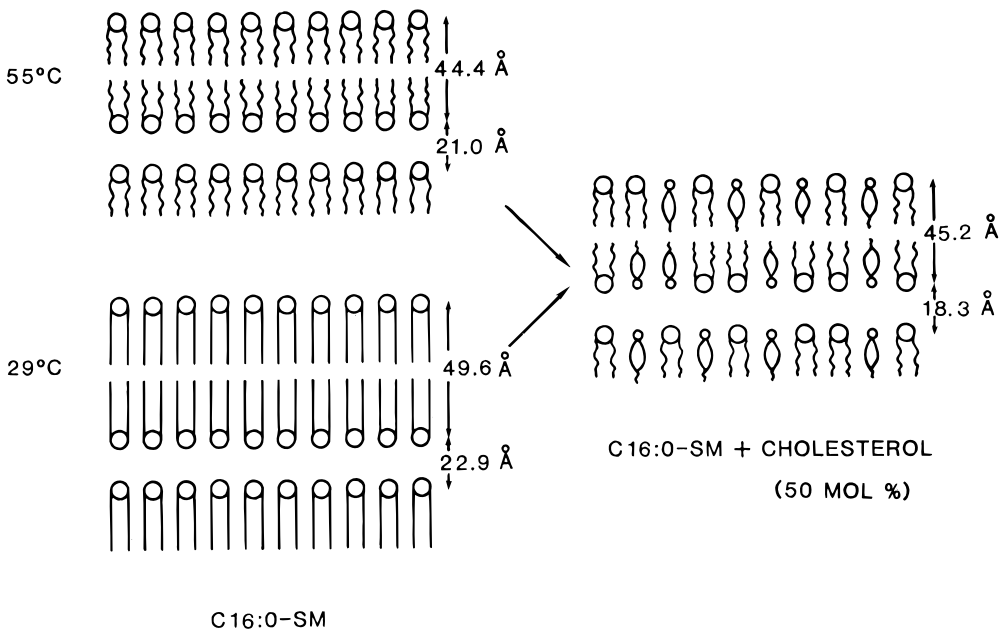

FIGURE 13: Effect of cholesterol on the bilayer structural parameters of hydrated C16:0-SM. The structural parameters shown are derived from the electron density profiles. The precise lateral packing arrangement of C16:0-SM and cholesterol within a monolayer is not known and is shown schematically.

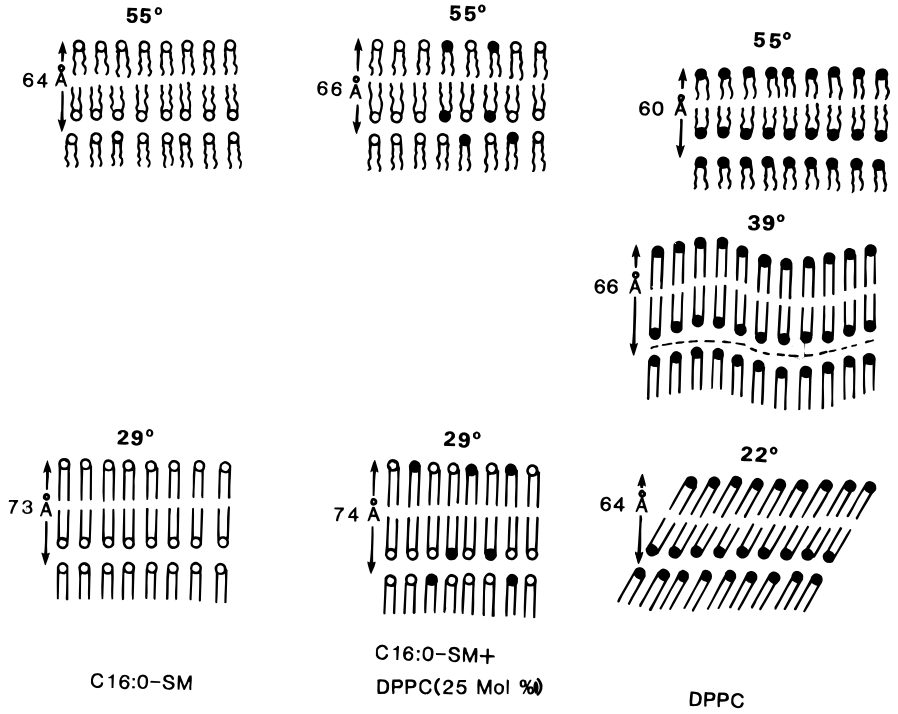

FIGURE 14: Schematic representation of the bilayer interactions of DPPC with hydrated C16:0-SM. Bilayer periodicities are shown.

by 4−5 Å (see data at 29 °C), whereas a small increase in bilayer thickness (∼1 Å) is observed compared to the liquid-crystal L_α phase of C16:0-SM alone. At 50 mol % cholesterol the bilayer thickness, d_{p-p}, is 45 Å, a value intermediate between those of the gel (∼50 Å) and liquid-crystal (∼44 Å) phases of C16:0-SM.

In addition, we note that, on the basis of the electron density profiles (Figure 10), the presence of 50 mol % cholesterol results in a small (3−4 Å) reduction of the inter-bilayer water thickness. Inter-bilayer hydration and the resulting thickness of this hydration layer are controlled by inter-bilayer forces. This balance of attractive and repulsive forces is determined by the molecular details of the interfacial lipid polar group and the properties of the inter-bilayer water. Some studies report a significant increase in PC bilayer hydration with cholesterol incorporation (Rand et al., 1980), whereas other studies show little or no effect (McIntosh et al., 1989). Recent studies of C24:0-SM/cholesterol hydration by McIntosh and co-workers (1992b) show a small reduction in inter-bilayer water thickness when comparing gel phase C24:0-SM with equimolar C24:0-SM/cholesterol at low applied pressures, in basic agreement with the effects described here for C16:0-SM/cholesterol. These data suggest that the presence of cholesterol alters the structure of the SM−water interface such that inter-bilayer forces are modified leading to a slight reduction of the hydration layer thickness. However, neither the structural basis of any interfacial alteration nor the specific repulsive or attractive

force(s) affected has been defined at this stage.

Thus, our present data confirm that cholesterol interacts with C16:0-SM bilayers, reducing and eventually removing the gel to liquid-crystalline transition of C16:0-SM; in addition, we provide details of the cholesterol-induced structural changes in C16:0-SM bilayers as shown schematically in Figure 13. While there is strong evidence supporting the orientation of cholesterol in the bilayer (with the hydroxyl group at the lipid−water interface) shown in Figure 13, the lateral packing arrangement of SM and cholesterol is not well defined.

C16:0-SM/DPPC Interactions. Our DSC (Figures 11 and 12) and X-ray diffraction data (not shown) confirm that DPPC is miscible with C16:0-SM in both its gel and liquid-crystal phases at all molar ratios. The bilayer structures exhibited by C16:0-SM, DPPC, and a typical binary mixture (25 mol % DPPC) are shown schematically in Figure 14. Interestingly, while the data show that C16:0-SM progressively destabilizes the Pβ' phase of DPPC present between the pre-transition and chain-melting transition, both the DSC data (Figures 11 and 12) and the X-ray diffraction data (not shown) suggest that up to ∼30 mol % C16:0-SM can be incorporated into the rippled Pβ' phase characteristic of DPPC.

The chain-melting temperatures of C16:0-SM and DPPC are similar (41−42 °C), and, perhaps predictably, there is no evidence of phase separation. Indeed, an earlier study (Calhoun & Shipley, 1979b) had shown miscibility of C16:0-SM with the lower melting DMPC (T_M = 23 °C). In contrast, we have shown previously that while bovine brain SM and egg yolk PC are completely miscible at high temperatures, they do undergo lateral phase separation of the higher melting SM component as the temperature is lowered (Untracht & Shipley, 1977). Thus, while SM and PC do have the ability to phase separate, if their chain-length and chain-melting temperatures are not too dissimilar, miscibility is observed in both the gel and liquid-crystal bilayer phases as clearly demonstrated here for C16:0-SM and DPPC.

ACKNOWLEDGMENT

We thank Dr. P. K. Sripada for the synthesis of C16:0-SM and Dr. David Atkinson for helpful advice. We also thank Ms. Irene Miller for assistance in preparing the manuscript.

REFERENCES

Barenholz, Y., Suurkuusk, J., Mountcastle, D. B., Thompson, T. E., & Biltonen, R. L. (1976) *Biochemistry 15*, 2441−2447.
Berridge, M. J., & Irvine, R. F. (1989) *Nature 341*, 197−205.
Bruzik, K. S. (1988) *J. Chem. Soc., Perkin Trans.* 423−431.
Bruzik, K. S., & Tsai, M.-D. (1987) *Biochemistry 26*, 5346−5368.
Calhoun, W. I., & Shipley, G. G. (1979a) *Biochim. Biophys. Acta 555*, 436−441.
Calhoun, W. I., & Shipley, G. G. (1979b) *Biochemistry 18*, 1717−1722.
Demel, R. A., Jansen, J. W. C. H., van Dijck, P. W. M., & van Deenen, L. L. M. (1977) *Biochim. Biophys. Acta 465*, 1−10.
Dong, Z., & Butcher, J. A. (1993) *Chem. Phys. Lipids 66*, 41−46.
Elder, M., Hitchcock, P. B., Mason, R., & Shipley, G. G. (1977) *Proc. R. Soc. (London) 252*, 4449−4457.
Elliott, A. J. (1965) *J. Sci. Instrum. 42*, 312−316.
Estep, T. N., Mountcastle, D. B., Barenholz, Y., Biltonen, R. L., & Thompson, T. E. (1979) *Biochemistry 18*, 2112−2117.
Estep, T. N., Freire, E., Mountcastle, D. B., Barenholz, Y., Biltonen, R. L., & Thompson, T. E. (1981) *Biochemistry 20*, 7115−7119.
Exton, J. H. (1994) *Biochim. Biophys. Acta 1212*, 26−42.
Franks, A. (1958) *Br. J. Appl. Phys. 9*, 349−352.
Hannun, Y. A. (1994) *J. Biol. Chem. 269*, 3125−3128.
Hannun, Y. A., & Obeid, L. M. (1995) *Trends Biochem. Sci. 20*, 73−77.
Hitchcock, P. B., Mason, R., Thomas, K. M., & Shipley, G. G. (1974) *Proc. Natl. Acad. Sci. U.S.A. 71*, 3036−3040.
Huang, C. (1991) *Biochemistry 30*, 26−30.
Janiak, M. J., Small, D. M., & Shipley, G. G. (1979) *J. Biol. Chem. 254*, 6068−6078.
Kratzer, B., Mayer, T. G., & Schmidt, R. R. (1993) *Tetrahedron Lett. 34*, 6881−6884.
Lin, H. N., Wang, Z. Q., & Huang, C. H. (1990) *Biochemistry 29*, 7063−7072.
Lin, H. N., Wang, Z. Q., & Huang, C. H. (1991) *Biochem. Biophys. Acta 1067*, 17−28.
Luzzati, V. (1968) in *Biological Membranes* (Chapman, D., Ed) pp 71−123, Academic Press, London.
Maulik, P. R., & Shipley, G. G. (1995) *Biophys. J. 69*, 1909−1916.
Maulik, P. R., Atkinson, D., & Shipley, G. G. (1986) *Biophys. J. 50*, 1071−1077.
Maulik, P. R., Sripada, P. K., & Shipley, G. G. (1991) *Biochim. Biophys. Acta 1062*, 211−219.
McIntosh, T. J., & Simon, S. A. (1986) *Biochemistry 25*, 4058−4066.
McIntosh, T. J., Magid, A. D., & Simon, S. A. (1989) *Biochemistry 28*, 17−25.
McIntosh, T. J., Simon, S. A., Needham, D., & Huang, C. (1992a) *Biochemistry 31*, 2012−2020.
McIntosh, T. J., Simon, S. A., Needham, D., & Huang, C. (1992b) *Biochemistry 31*, 2020−2024.
Nagle, J. F., & Wilkinson, D. A. (1978) *Biophys. J. 23*, 159−175.
Nishizuka, Y. (1984) *Nature 308*, 693−698.
Oldfield, E., & Chapman, D. (1971) *Biochem. Biophys. Res. Commun. 43*, 610−616.
Oldfield, E., & Chapman, D. (1972) *FEBS Lett. 21*, 303−306.
Pearson, R., & Pascher, I. (1979) *Nature 281*, 499−501.
Rand, R. P., Parsegian, V. A., Henry, J. A. C., Lis, L. J., & McAlister, M. (1980) *Can. J. Biochem. 58*, 959−968.
Reiss-Husson, F. (1967) *J. Mol. Biol. 25*, 363−382.
Seelig, J., & Seelig, A. (1980) *Q. Rev. Biophys. 13*, 19−61.
Shapiro, D., & Flowers, H. M. (1962) *J. Am. Chem. Soc. 84*, 1047−1050.
Shipley, G. G., Avecilla, L. S., & Small, D. M. (1974) *J. Lipid. Res. 15*, 124−131.
Sripada, P. K., Maulik, P. R., Hamilton, J. A., & Shipley, G. G. (1987) *J. Lipid Res. 28*, 710−718.
Torbet, J., & Wilkins, M. H. F. (1976) *J. Theor. Biol. 62*, 447−458.
Untracht, S. M., & Shipley, G. G. (1977) *J. Biol. Chem. 252*, 4449−4457.
van Dijck, P. W. M., de Kruijff, B., van Deenen, L. L. M., de Gier, J., & Demel, R. A. (1976) *Biochim. Biophys. Acta 455*, 576−587.
Worthington, C. R., & Blaurock, A. E. (1969) *Biophys. J. 9*, 970−990.

BI9528356